Classification
*Physics Abstracts*
61.14 — 61.14D — 61.14R

# The HOLZ lines in Si[111] zone axis patterns

Gottfried Möllenstedt and Fang Zhou

Institute of Applied Physics, University of Tübingen, Auf der Morgenstelle 12, 7400 Tübingen 1, Germany

*(Received January 29, 1992; accepted April 21, 1992)*

**Abstract.** — High order Laue zone (HOLZ) lines in the high symmetry zone axis of Si[111] have been carefully examined theoretically and experimentally. The dependences of the displacement of HOLZ lines in Si[111] zone axis patterns on the incident electron energy and on the lattice parameter were studied using computer simulations based on the Bloch wave many beam theory. Thus, the angular displacement of HOLZ lines was found to vary with voltage at a rate of 0.24 mrad/kV at about 100 kV. The HOLZ lines $(\bar{5}, \bar{5}, 11)$, $(\bar{5}, 11, \bar{5})$ and $(11, \bar{5}, \bar{5})$ were found to coincide at an incident electron energy of 103.15 keV. Experimental convergent beam electron diffraction (CBED) patterns obtained using an electron microscope equipped with either a field emission gun (FEG) or an energy filter are compared with computer simulations. Good agreement between experimental and simulated patterns is found if the electron energy is adequately corrected for materials with known lattice parameters. The high precision of lattice parameter determinations using the coincidences of X-rays from lattice sources according to Walther Kossel and the accurate material analysis using Castaing's microprobe are mentioned in this context.

## 1. Preface.

Microanalysis using the Castaing X-ray microprobe [1] was described by Professor Guinier at the occasion of Castaing's nomination as a member of the Academie Française and the "Remise d'Epée d'Académicien" in Paris in June 1978 with the following impressive words:

*Ce n'est certes pas simple de symboliser dans un dessin une oeuvre scientifique. Mais l'artiste à qui est due cette épée a su évoquer par un graphisme élégant et simple le principe de la sonde de Castaing. Des électrons se précipitent sur un point de l'objet d'où s'échappent les rayonnements qui portent en eux la nature intime de la matière touchée quand on les soumet à l'analyse spectrale dont un arc-en-ciel nous rappelle la manifestation la plus naturelle.*

Castaing's method is based on the production of an electron microprobe with the smallest possible diameter. If it is directed onto the material to be studied, characteristic X-ray radiation is released which is analyzed using a spectrometer of high precision. Castaing's microprobe has won worldwide reputation as a valuable modern analytic tool for the analysis of extremely small volume elements.

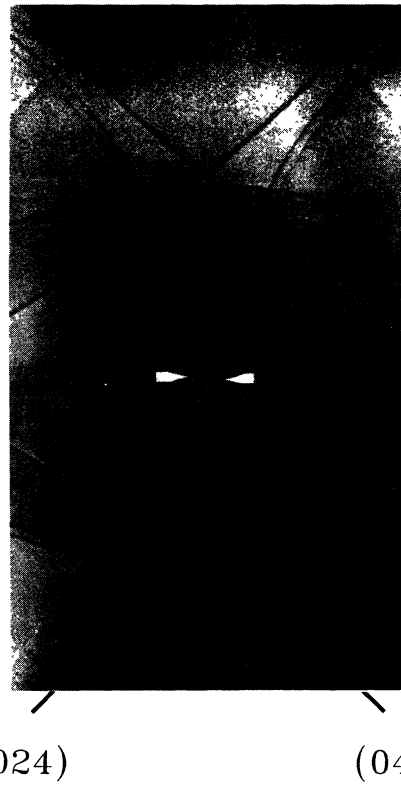


Fig. 1. — The emission from a Cu-monocrystal-anticathode. The distance from crystal to photoplate is 20 cm.

The Faculty of Mathematics and Natural Sciences of the Eberhard-Karls University at Tübingen conferred to Prof. Dr. Raimond Castaing the title of an honorary doctor of natural sciences appreciating the ingenious creator of material selective imaging using X-ray and ions.

## 2. Introduction.

2.1 COINCIDENCE OF X-RAY INTERFERENCES — Before discussing the coincidence of HOLZ lines in CBED patterns, we should like to make some remarks on the coincidence of X-ray interferences according to Walther Kossel [2-4].

X-ray interferences from lattice sources are produced if monocrystals are irradiated by electrons. Due to Bragg reflections, interference lines are recorded on a distant photographic plate. Figure 1 shows the emission from the region close to the rhombic dodecahedral pole of a monocrystalline copper anticathode. The arrows show that the interferences (024) and (042) approach each other down to a small angle. Kossel used this coincidence for a precise determination of lattice parameters.

In terms of the conventional spectrometric concepts, this method of using the coincidence of reflections from different lattice planes can be understood as follows:

The problem consists in measuring $\lambda/a$ as the sine of a diffraction angle. Thus, every spectrometer is essentially an instrument for measuring angles, and all diligence applied to alignment and graduation is directed towards this aim. In the crystals a number of lattices capable of producing spectra are positioned in a precise well defined orientation with respect to each other. These

angles supplied by nature are used as standards for the diffraction angles to be measured. The precision instrument supplied by nature is working with an accuracy which can be equalled by the artificial angular graduation of a spectrometer only if extreme precision in the construction and a high amount of experience and diligence in its application are attained.

Examples for the application of Kossel's coincidence method were given by van Bergen [3] who determined the lattice parameter of Cu, $a = 3607.53 \pm 0.04\ XE$ at 20 °C using the precise knowledge of the wave lengths of the $K_\alpha$ lines. This is a precision of $\Delta d/d = 1.11 \times 10^{-5}$. Similar measurements for Zn were made by Anker [4].

2.2 COINCIDENCE OF HOLZ LINES IN CBED PATTERNS — Similar to the phenomenon of coincidence of X-ray interference, the coincidence of high-order Bragg reflections in CBED patterns was observed by Steeds *et al.* [5]. While lattice parameters could be measured with high precision using the coincidence of X-ray interference lines, the coincidence of electron interferences according to Steeds allows to determine the electron wavelength and hence the accelerating voltage of electrons if the lattice parameters are known. Making use of the coincidence of three high-order Bragg reflections in electron diffraction is an elegant method for the experimental physicist.

The position of HOLZ lines is sensitive to small changes in lattice parameter and microscope voltage. Steeds *et al.* [5] used the positions of HOLZ lines in Si[111] to determine the accelerating voltage of the electron microscope. It was found that the positions of kinematically simulated HOLZ lines do not match the experimental patterns [6].

The dynamical theory of electron diffraction instead of the kinematical theory is used to simulate the zone axis patterns. The three-dimensional potential distributions in crystals and the anomalous absorption effect are taken into account. The HOLZ lines and their corresponding reflections may be directly simulated. Simultaneously the specimen thickness and the energy of incident electrons are precisely determined. The accuracy which can be attained in connection with computer simulation will be discussed in the following.

## 3. Experiment.

The HOLZ patterns were observed using the CBED method on a Philips EM 420 electron microscope equipped with a field emission gun (FEG) and on a Zeiss EM 912 equipped with an "Omega" magnetic imaging energy filter. In order to study the sensitivity of the position of HOLZ lines in the bright field disc of zone axis patterns with respect to voltage variations it was necessary to be able to vary continuously the accelerating voltage of the microscope. CBED patterns of very high quality could be obtained if the background formed by inelastically scattered electrons was removed using the Omega energy filter. Thus, hitherto not observable details become visible such as the very fine narrow fringes in the $(2\bar{2}0)$ reflection marked by an arrow in figure 4. We shall report later on successful attempts to explain this phenomenon by computer simulation. The advantage of the FEG is that it can supply a highly mono-energetic and very bright electron source. Thus, an electron probe of small diameter can be easily formed on the surface of the specimen, and more detailed structures in the CBED patterns can be obtained with less energy spread of the incident electrons. Cold-stages were used in both electron microscopes to prevent serious contamination in the experiment.

Most work was done on Si [111] and [001] single crystal specimens thinned by ion-milling. Patterns were taken at various voltage settings in the vicinity of 100 kV.

## 4. Theory and computer-simulation.

A set of programs based on the Bloch wave theory of dynamical electron diffraction established by Bethe [7] was developed. Using this program we can simulate zone axis patterns, two-dimensional CBED patterns, Kikuchi maps, line-scans etc. The absorption effect may be taken into account by solving a complex matrix equation instead of using perturbation approximation theory [8,10]. A detailed description of these programs will be given in a separate paper. Reviews of the many-beam Bloch wave theory may be found in references [8,9]. In the present paper, only the basic assumptions and some important clues for solving the problem will be briefly mentioned. The specimen is assumed to be a thin parallel-sided ideal slab crystal without defect. This is a reasonable assumption if the electron beam is focused into a sub-micron region of the specimen. Thus, incident electrons are scattered by a three-dimensional periodic lattice potential field which can be written as a Fourier series. The wave function of the incident electron within the crystal is represented by a linear superposition of a finite number of Bloch waves. Thus, the problem consists in solving Schrödinger's equation for the three-dimensional lattice potential $V(\mathbf{r})$. Spin effects are neglected. It is further assumed that the high energy approximation is applicable ($E \geq 70$ keV), that the zone axis is perpendicular to the crystal surface, and that the angle between the wave vector of the incident electrons and the zone axis is small. Then the problem of solving Schrödinger's equation is reduced to the solution of an eigenvalue problem for a matrix the rank of which is determined by the number of Bloch waves taken into account. HOLZ reflections may be included. A non-orthogonal linear transformation is needed to transform the resulting matrix into an Hermitian shape [5]. The possible Bloch waves associated with wave-vectors $\mathbf{K}^{(j)}$ and amplitudes $C_{\mathbf{g}}^{(j)}$ are obtained by solving the matrix equation. Finally, the excitation amplitudes $\alpha^{(j)}$ of every Bloch wave are determined from the condition that the tangential components of the Bloch waves must satisfy the condition of continuity at the crystal boundary. Inelastic scattering processes may be taken into account by adding an imaginary part $iV'(\mathbf{r})$ to the real potential. In this case the matrix equation to be solved is complex.

Computer simulations were made by using standard routines for the solutions of eigenvalue equations in the NAG (Numerical Algorithms Group) library. The routine F02ABF was used to solve a real symmetric matrix equation whereas the routine F02AKF was used to solve a general complex matrix equation. Results obtained using different routines will be discussed later. The Si crystal has a centrosymmetric structure. If the origin of the unit cell is placed at the bonding center, and if absorption is neglected then the matrix becomes real and symmetric. The computer time needed to solve a real symmetric matrix equation is shorter by a factor of three or four as compared to the solution of a general complex matrix equation of the same rank.

Up to 100 beams could be taken into account with our program. In practice the number of beams is restricted in order to prevent the matrices from becoming too large to be easily manageable. In order to save computer time we admit only such reciprocal lattice points for which the modulus of the structure potential is relatively large and which are close to the Ewald sphere of radius $K = |\mathbf{K}|$, i.e. the wave number of the incident electron corrected for the mean potential. Thus, reflections in the first or even second Laue zone may be included.

We have used the low index structure potentials of Si determined experimentally by Voss and Lehmpfuhl [11] which are believed to be in excellent agreement with data from accurate X-ray diffraction by Aldred and Hart [12]. The structure potentials which were not available from the experimental results in [11] were obtained using both atomic scattering amplitudes for X-rays and for electrons in [13]. Such atomic scattering factors at high angles as tabulated in [14] must be included if HOLZ lines or very high-order reflections are taken into account in the calculations. The structure potentials were corrected using the temperature factor $\exp\{-B(\sin\theta/\lambda)^2\}$ where

the coefficient $B = 0.4613$ Å$^2$ [12] is used for Si at room temperature. For other specimen temperatures the value of B was derived theoretically using a method [15] applicable only to cubic crystals formed by only one kind of atom. For the mean potential of Si the value of $V_0 = 11.5$ V [12] is used.

When absorption was taken into account, the imaginary part of the structure potentials was, for non-vanishing g, determined according to [11]

$$V'_g = V_g(b \mid \mathbf{g} \mid -c \mid \mathbf{g} \mid^2) \tag{1}$$

where g is the reciprocal lattice vector, $\mid \mathbf{g} \mid = 2\pi/d_{hkl}$, $b = 0.004$ Å and $c = 0.0003$ Å$^2$ [11]. The mean absorption potential is, $V'_0 = 0.61$ V. Instead of equation (1) we have alternatively used

$$V'_g = CV_g \tag{2}$$

with constant $C = 0.03$-$0.05$. These $V'_g$ values are valid for 100 keV incident electrons. For other electron energies, the correction used by Humphreys and Hirsch [16] was applied.

The lattice parameter of Si, $a = 5.4307$ Å and the coefficient of linear expansion, $\alpha = 3 \times 10^{-6}$ $(°C)^{-1}$ ( at 25 °C ) [17] was used in the calculation. The Debye temperature for Si used in the calculation of the temperature coefficient $B$ is 625 K [17].

Relativistically corrected values of the electron mass $m$ and the wave length $\lambda$ were used in the computer simulation.

## 5. Zone axis pattern and HOLZ lines.

CBED patterns contain three-dimensional information on the material. They are formed if a thin crystal is irradiated by a convergent conical electron beam[18]. In a single CBED pattern reflections of zero and higher order Laue zones may be excited. The excited high order reflections produce dark HOLZ lines in the bright field disc, and circles formed by reflections associated with high order zones. If the cone axis of the incident electron beam is parallel with a zone axis, then we obtain a highly symmetric zone axis pattern.

Figure 2a is a Si[111] zone axis pattern recorded with the Philips EM420 at 100 kV. Figure 2b shows a computer simulated zone axis pattern of Si[111] for the same experimental conditions in which absorption effects were taken into account using equation (2) with $C = 0.04$. The agreement between the calculated dark field disc patterns and the experimental results is poorer if the smaller imaginary part $iV'(\mathbf{r})$ of the potential following from equation (1) is used. Figure 3 is a computer simulated short camera length zone axis pattern of Si[111] at 100 kV. Figure 4 represents a Si[111] zone axis pattern recorded with the Zeiss EM912 at 102.7 kV. The slight distortion of the pattern is due to deviations from the assumed ideal symmetry such as misalignment or asymmetries of the illuminating cone or as deviations of the real crystal shape from the ideal one. The approximately hyperbolic splitting of the HOLZ lines observed close to the intersection of their asymptotes is observed in both the experimental pictures and in the simulations (cf. Figs. 2a, 4 and 2b). It is found that the splitting is wider at lower crystal temperatures because the structure potentials are greater than those at higher temperatures due to the Debye-Waller factor. The same is true for splittings of intersecting HOLZ lines and rings, i.e. the zero zone pattern.

HOLZ lines may be observed in each of the $(\bar{2}20)$ dark field discs both in experimental patterns and in their simulations which show very good agreement. In addition, calculations indicate that reflections of high order Laue zones exert only very weak influence on the zero zone pattern, i.e. the ring system.

The interactions among different reflections are caused by dynamical effects. They can be perfectly simulated using the many beam Bloch wave theory.

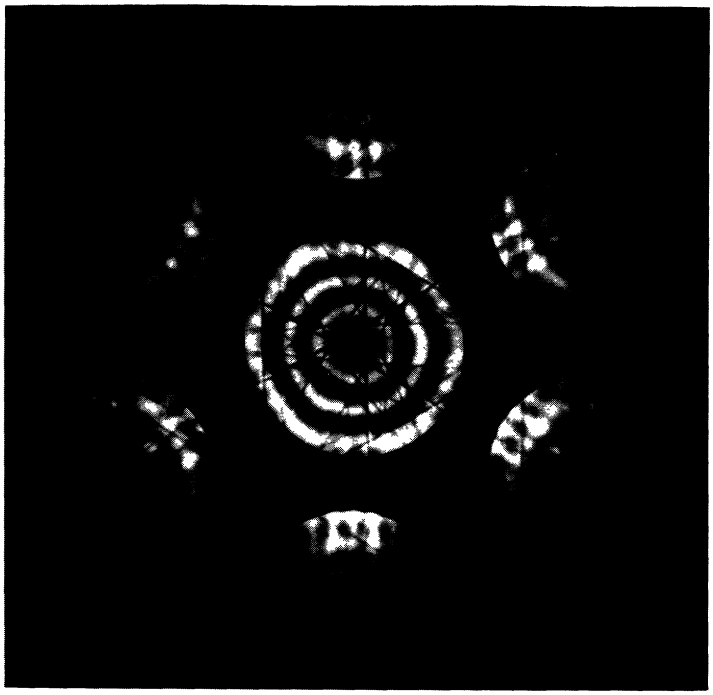

a)

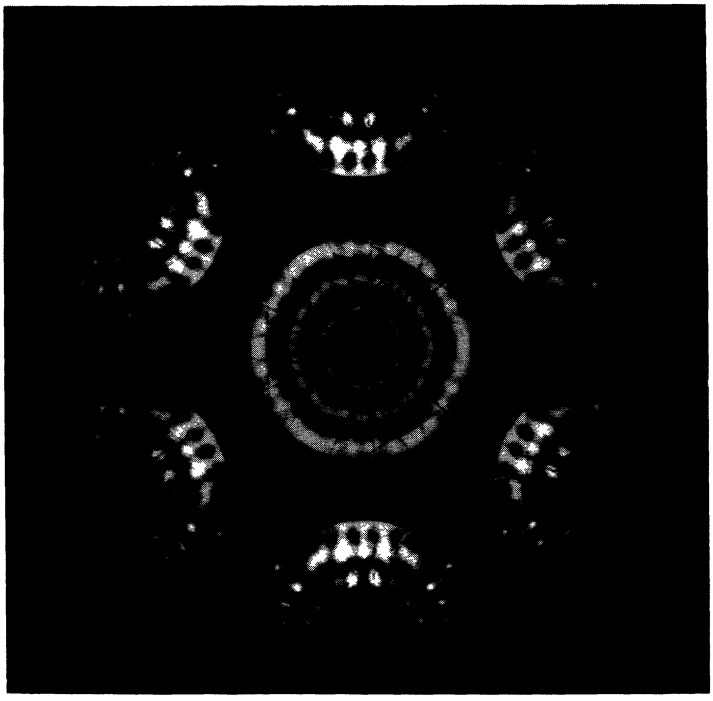

b)

Fig. 2. — a) Experimental Si[111] zone axis pattern at 100 kV; 300 K; $D = 1855$ Å; with FEG. b) Computer simulated Si[111] zone axis pattern under the same conditions as figure 2a; 55 beams; $C = 0.04$.

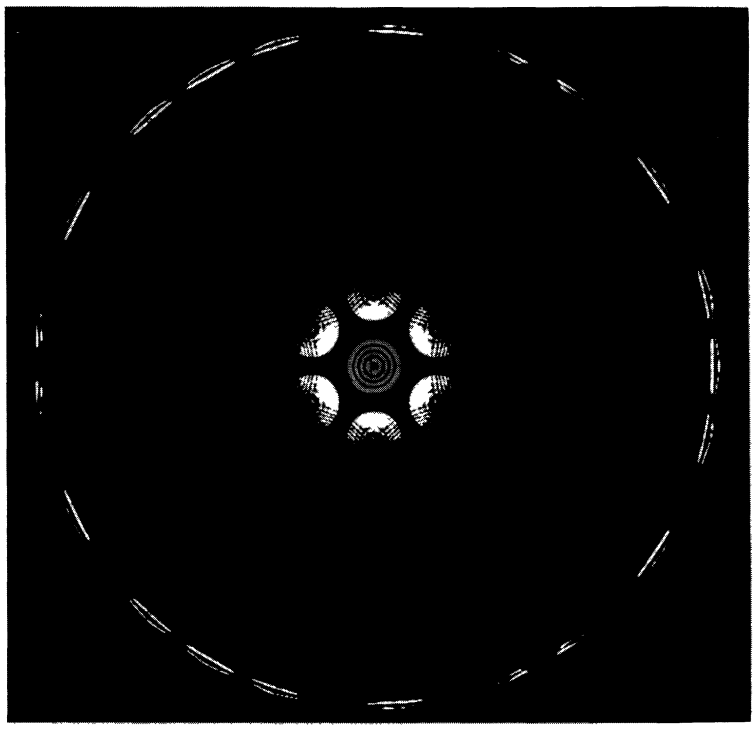

Fig. 3. — Simulated short camera Si[111] zone axis pattern at 100 kV; $D = 3000$ Å; 300 K; $C = 0.04$; 67 beams.

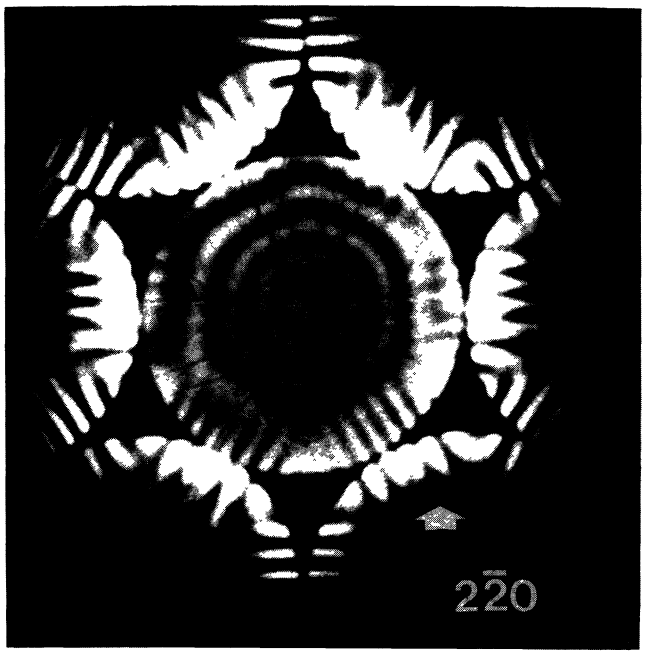


Fig. 4. — Si[111] zone axis pattern recorded with "Omega" energy filter at 102.7 kV; $D = 2160$ Å; 300 K. The arrow in reflection disc ($2\bar{2}0$) indicates the position where the very fine fringe structure is found.

## 6. The sensitivity of HOLZ line shift.

The position of HOLZ lines depends sensitively on the initial energy of the incident electrons and on the lattice parameter. According to the kinematic theory, this dependence is described as follows:

$$\frac{d\theta}{dU} = -\frac{|g|}{4U} \cdot \frac{(1+2\epsilon U)}{(1+\epsilon U)} \cdot (K^2 - \frac{|g|^2}{4})^{-\frac{1}{2}} \tag{4}$$

$$\frac{d\theta}{da} = -\frac{|g|}{2a} \cdot (K^2 - \frac{|g|^2}{4})^{-\frac{1}{2}} \tag{5}$$

In these equations $\theta$ is the angular displacement of the HOLZ line indexed by the reciprocal lattice vector g, and | g | is the modulus of g, $U$ is the accelerating voltage of the microscope, $a$ the lattice parameter, $K$ the wave vector corrected for the mean potential, and $\epsilon := \frac{e}{2m_0c^2} = 9.7846 \times 10^{-7}$ $V^{-1}$. It should be noted that equation (4) is applicable to cubic crystals only. Equations (3) and (4) indicate that the HOLZ line shift increases with increasing | g | and with decreasing $U$. For the HOLZ line $(\bar{5},\bar{5},11)$ in the Si[111] bright field disc of the zone axis pattern at 100 kV, we have $|\frac{d\theta}{dU}| \approx 0.2429$ mrad/kV and $|\frac{d\theta}{da}| \approx 8.21$ mrad/Å.

The dynamical many beam calculation with our program yields good agreement with the kinematically estimated value for $|\frac{d\theta}{dU}|$. Figure 5 shows the shift of the $(\bar{5},\bar{5},11)$ HOLZ line if the electron energy is varied from 100 keV to 101 keV. The value of $|\frac{\Delta\theta}{\Delta U}|$ derived from this dynamical simulation is $|\frac{\Delta\theta}{\Delta U}| \approx 0.2383$ mrad/kV. Figure 6 shows the displacement of the $(\bar{5},\bar{5},11)$ HOLZ line if the temperature of the crystal is varied from 300 K to 100 K. The corresponding variation $\Delta a$ of the lattice parameter is $3.26 \times 10^{-3}$ Å, the resulting value of $|\frac{\Delta\theta}{\Delta a}| \approx 14.889$ mrad/Å is much greater than the kinematically estimated value. The reason for this discrepancy

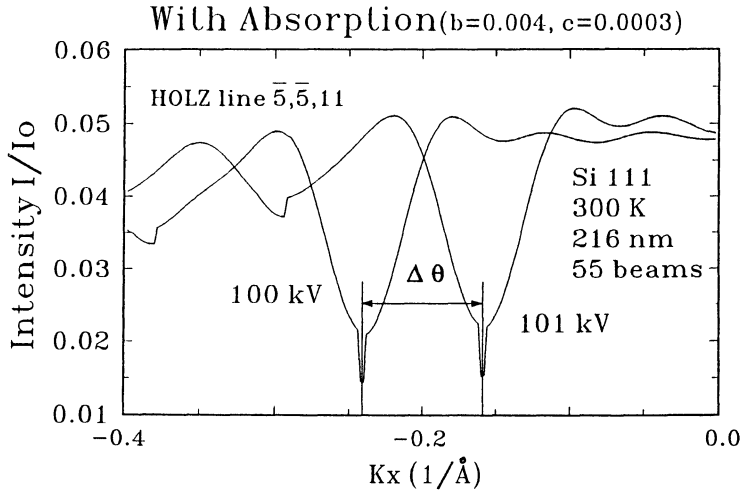


Fig. 5. — The positions of the HOLZ line $(\bar{5},\bar{5},11)$ at 100 kV and 101 kV.

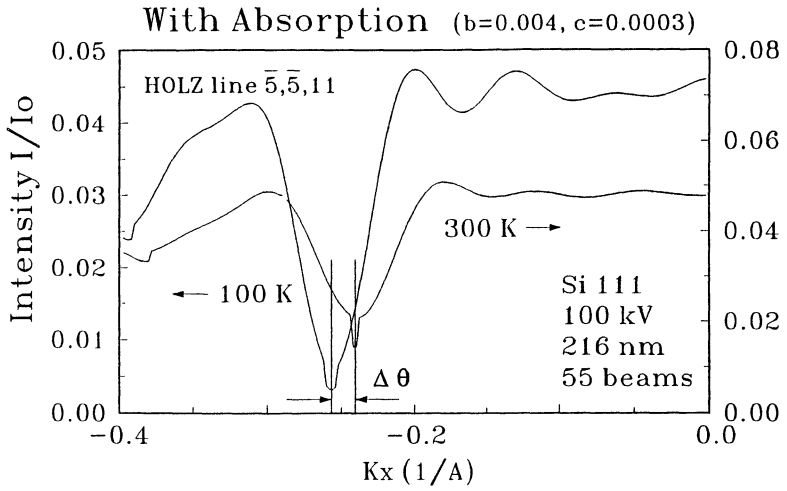


Fig. 6. — The positions of the HOLZ line $(\bar{5}, \bar{5}, 11)$ at the temperatures of 300 K and 100 K.

is that the kinematically estimation takes into account only the variation of the lattice parameter but not the temperature and lattice parameter dependence of the structure potentials. For this reason the dependence of the position of the HOLZ lines on temperature is not well enough described by the kinematical theory, but a better description may be expected from dynamical simulations.

Further calculations showed that the position of HOLZ lines does not depend much on whether the absorption effect is taken into account or not. Actually the additional line shift due to the absorption effect was less than the HOLZ line width, as shown in figure 7. Thus, when calculating

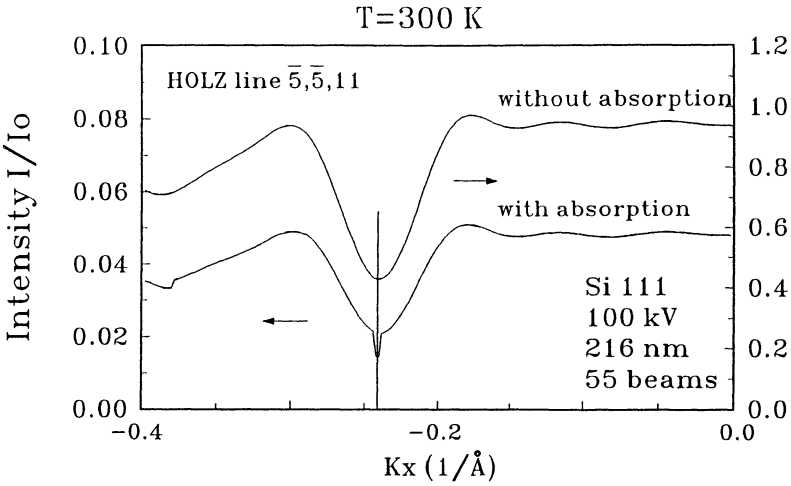


Fig. 7. — The calculated positions of the HOLZ line $(\bar{5}, \bar{5}, 11)$ with and without absorption effect.

the position of the HOLZ lines we may neglect the absorption and thus save much computer time since the solution of the real matrix equations is much faster than that of the general complex one. Let us now estimate the accuracy with which the microscope voltage and the lattice parameter can be measured by observing the shift of HOLZ lines. In order to attain an angular resolution of 0.015 mrad, the point resolution must be better than 15 $\mu$m for a camera length of 1000 mm. The voltage variation corresponding to a shift of 0.015 mrad is $\Delta U \approx 62$ V at about 100 kV.

Making use of small angle intersections of lines moving in different directions [5] may improve the accuracy of voltage and lattice parameter measurements. In order to attain high sensitivity it is also suggested to select a HOLZ line with large | g |.

## 7. Coincidence of HOLZ lines.

In the experiment we observed that HOLZ lines $(\bar{5},\bar{5},11)$, $(\bar{5},11,\bar{5})$ and $(11,\bar{5},\bar{5})$ intersect in a point instead of a triangle in the center of the bright field disc at about 102.7 to 102.8 kV (cf. Fig. 4). According to the kinematical theory this should occur for 101.72 kV, i.e. if the excitation error vanishes:

$$| \mathbf{K} | - | \mathbf{K} + \mathbf{g} | = 0 \tag{5}$$

| K | is again corrected for the mean potential.

The dynamical simulation yields a coincidence voltage of 103.15 kV. Figure 8 shows the bright field pattern for 102 kV and 103.15 kV and a voltage dependent intensity distribution of line-scans across the middle of the bright field disc. A more precise calculation over a small range of $K_x$ values similar to the simulation represented in figures 5 and 6 confirms this result.

It was found in many experiments that the positions of the observed HOLZ lines in various zone axes of various crystals deviated slightly from the positions predicted by the kinematical theory [6]. In our case, i.e. at about 100 kV , the corresponding voltage deviation was $\Delta E = (103.15 - 101.72)\ kV = 1.43\ kV$.

## 8. Thickness of the specimen

The bright field disc of the zone axis pattern shows a number of concentric rings the number of which depends on the crystal thickness. A new ring appears when the specimen thickness increases by one extinction length which can be calculated quite accurately. The specimen thickness may be obtained by comparing the experimental picture with figure 9 which shows the thickness-dependent intensity distribution of line-scans across the middle of the bright field disc at 100 kV. The thickness can be determined with an accuracy of about 20 Å by the number of rings and the relative positions of HOLZ lines and rings. The extinction length in direction of the Si[111] zone axis is 239 Å at 100 kV. Its value depends not only on $V_{220}$ but also on other structure potentials. Thus, it is markedly different from the extinction length of the reflection (220) of 79.1 Å at 100 kV. If absorption is taken into account, then the intensity in the center of the bright field disc decreases more rapidly with crystal thickness than at points near to its periphery which are closer to the Bragg position of the $(\bar{2}20)$ reflections. Our calculations show that the absorption has practically no effect on the positions of the rings in the ring system in the bright field disc. The simulated intensity distribution in the $(\bar{2}20)$ dark field disc is in good agreement with the experimental result only if absorption is taken into account.

The dynamical calculations show that the HOLZ line positions are essentially independent of the crystal thickness whereas the width of the HOLZ lines depends on the thickness. Sufficiently narrow HOLZ lines are observed for thicknesses between 2000 and 3000 Å which seem to be

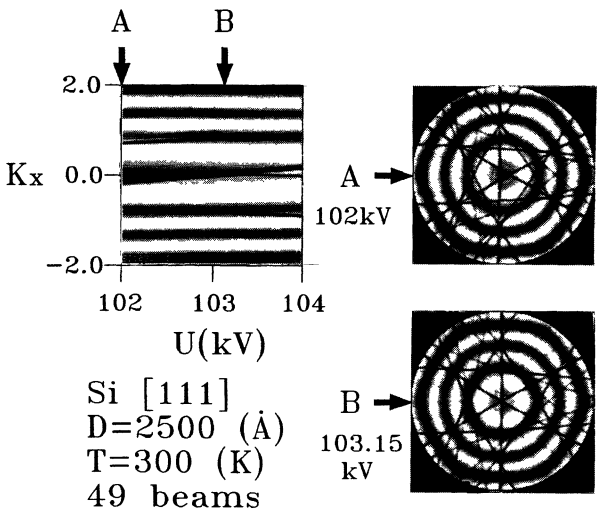


Fig. 8. — The electron energy dependent line-scans across the middle of the bright field disc, 102 kV - 104 kV.

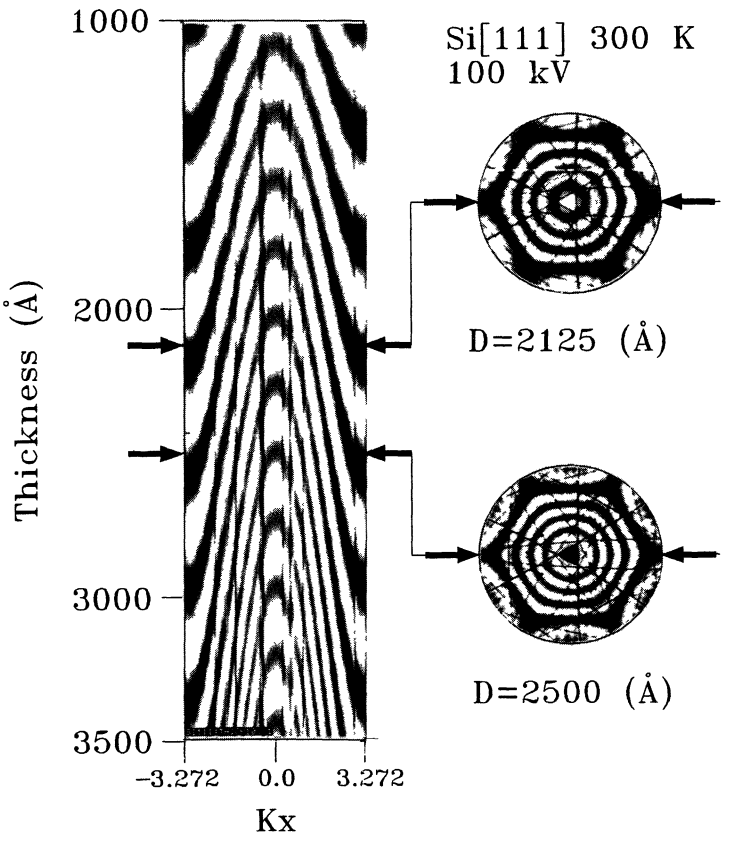


Fig. 9. — Thickness dependent line-scans across the middle of the bright field disc, 1000 Å - 3500 Å.

optimal for accurate measurements. Any further increase of thickness to 4000 Å and beyond does not improve the experimental conditions because of the diffuse scattering background in the experimental pattern and discontinuity of HOLZ lines by dynamical interaction with the ring system consisting of too many rings.

**Acknowledgments.**

We should like to express our thanks to the Deutsche Forschungsgemeinschaft for financial support with respect to material as well as personal costs. We wish to express our gratitude to Prof. F. Lenz, Prof. K.-H. Herrmann and Prof. H. Lichte for their interest and valuable suggestions. We thank Prof. F. Lenz for checking the English manuscript. We are also grateful to Dr. Mayer and Ms. Deininger at the Max-Planck-Institut für Metallforschung at Stuttgart for their help in using the Zeiss EM912 and for supplying the Si[111] specimen.

**References**

[1] CASTAING R., Application of electron probes to local chemical and crystallographic analysis, Thesis, Univ. of Paris, 1951.
[2] KOSSEL W., Röntgeninterferenzen aus Gitterquellen, *Ann. Phys.* **26** (1936) 533.
[3] VAN BERGEN H., Präzisionsmessung von Gitterkonstanten mit einer Kompensationsmethode, *Ann. Phys.* **33** (1938) 737.
[4] ANKER B., Präzisionsmessung der Gitterkonstanten, und Untersuchung von Gitterstörungen, *Ann. Phys. 6. Folge* **12** (1953) 1-3.
[5] JONES P.M., RACKHAM G.M. and STEEDS J.W., Higher order Laue zone effects in electron diffraction, and their use in lattice parameter determination *Proc., R. Soc. London A.* **354** (1977) 197-222.
[6] OKUYAMA T., MATSUMURA S., KUWANO N. and OKI K., Dynamical diffraction effects on higher-order Laue zone lines in CBED patterns of semiconductors, *Ultramicroscopy* **31** (1989) 309-318.
[7] BETHE H.A., Theorie der Beugung von Elektronen an Kristallen, *Ann. Phys. (Leipzig)* **87** (1928) 55-129.
[8] HUMPHREYS C.J., The scattering of fast electrons by crystals, *Rep. Prog. Phys.* **42** (1979) 1825.
[9] VALDRÈ U. and RUEDL E., Electron Microscopy in Materials Science (1976).
[10] BUXTON B.F., Bloch waves and higher order Laue zone effects in high energy electron diffraction, *Proc. R. Soc. London A.* **350** (1976) 335-361.
[11] VOSS R., LEHMPFUHL G. and SMITH P.J., Influence of doping on the crystal potential of silicon investigated by the convergent beam electron diffraction technique, *Z. Naturforsch.* **35a** (1980) 973-984.
[12] ALDRED P.J.E. and HART M., The electron distribution in silicon, *Proc. R. Soc. London Ser. A* **332** (1973) 223-254.
[13] International Tables for X-ray Crystallography, Volume IV (1974) pp. 71-102.
[14] DOYLE P. and TURNER A., Relativistic Hartree-Fock X-ray and Electron Scattering Factors, *Acta Cryst.* A **24**, (1968) 390.
[15] International Tables for X-ray Crystallography, Volume II (1985) p.241.
[16] HUMPHREYS C.J. and HIRSCH P.B. Absorption parameters in electron diffraction theory, *Philos. Mag. Vol.* **18** (1968) 115.
[17] Handbook of Chemistry and Physics, 58th edition (CRC Press, ed. 1977-1978 ).
[18] KOSSEL W. and MÖLLENSTEDT G., Elektroneninterferenzen im konvergenten Bündel, *Naturw.* **26** (1938) 660.